

Trapping of deformable active particles by a periodic background potentialJia-jian Li , Rui-xue Guo, and Bao-quan Ai**Guangdong Basic Research Center of Excellence for Structure and Fundamental Interactions of Matter,
Guangdong Provincial Key Laboratory of Quantum Engineering and Quantum Materials,
School of Physics, South China Normal University, Guangzhou 510006, China
and Guangdong-Hong Kong Joint Laboratory of Quantum Matter, South China Normal University, Guangzhou 510006, China* (Received 16 October 2023; revised 10 March 2024; accepted 20 March 2024; published 18 April 2024)

The dynamic behaviors, specifically trapping and sorting, of active particles interacting with periodic substrates have garnered significant attention. This study investigates numerically the trapping of soft, deformable particles on a periodic potential substrate, which can be experimentally verified through optical tweezers. The research demonstrates that multiple factors, including the relative size of traps, self-propelled velocity, shape parameters, ratio of particles to traps, and translational diffusion, can influence the trapping effect. Within certain parameter boundaries, it is shown that all particles can be consistently trapped. The research reveals that stable trapping typically occurs at median values of the relative trap size. An increase in the self-propelled velocity, the shape parameter, and the translational diffusion coefficient tends to facilitate the escapement of the particles from the traps. It is noteworthy that particles with larger shape parameters can escape even when the restoring force exceeds the self-propelled force. In addition, as the ratio of particles to traps grows, the fraction of trapped particles steadily reduces. Notably, rigid particles are consistently divided and trapped by traps closely approximating an integer multiple of the particles' area, up until the ratio reaches the aforesaid integer value. These findings can potentially enhance the understanding of the interactive effects between active deformable particles and periodic substrates. Moreover, this work suggests a different experimental approach to sort active particles based on rigidity disparities.

DOI: [10.1103/PhysRevE.109.044143](https://doi.org/10.1103/PhysRevE.109.044143)**I. INTRODUCTION**

Active particle systems, due to the injection of intrinsic energy, are far from equilibrium, thereby presenting a plethora of behavioral possibilities [1]. Over the years, a broad range of effects and dynamics, including the ratchet effects [2–7], collective motion [8,9], glasslike dynamics [10,11], and phase separation [12,13], have been extensively reported. Recently, significant attention has been directed towards the phenomena arising from the coupling of active particles with periodic substrates. These substrates may either resemble a periodic obstacle array or may replicate the egg-carton substrate observed in an optical tweezers' lattice. Noteworthy phenomena in this domain include dynamic locking or guidance in specific directions [14–16], anomalous diffusion [17,18], and trapping [19–22]. Of particular interest is the trapping phenomenon, as it paves the way for innovative approaches to segregate and sort particles based on their properties.

Prior research on particle trapping has largely focused on active disk particles, with relatively little attention granted to deformable particles constrained by deformation [19–22]. Nevertheless, these deformable particles are commonly observed in a range of settings, including cell monolayers [23], developing tissues [24], compressed foams [25], and emulsions [26]. The deformability of these particles notably

influences system behavior [27–36]. Questions remain as to whether a deformable particle can be adequately trapped by the periodic potential substrates and how its deformability might affect its trapping behaviors. These represent important open questions in the field.

To answer these open questions, we conducted a numerical investigation focusing on the trapping of active, deformable particles within a periodic potential substrate. Our findings illustrate that several factors significantly affect trapping outcomes, including the relative trap size, the self-propelled velocity of particles, shape parameters, ratio of particles to traps, and translational diffusion. Our investigation concludes that all the particles can be stably trapped within a specifically tailored parameter regime. Moreover, moderate values of trap size are quite conducive to stable particle trapping. Interestingly, we found that increasing the self-propelled velocity, shape parameters, and translational diffusion coefficient facilitates particle escape from traps, with particles possessing a larger shape parameter still able to escape traps, even when the self-propelled force is smaller than the restoring force. Strikingly, stiffer particles can be evenly distributed and securely maintained within traps that have an area close to an integral multiple of the particle area, until the ratio between the number of particles and traps increases to the above-mentioned integer value. Conversely, softer particles might escape when the ratio of particles to traps is lower. Our findings offer valuable insights into the dynamic behaviors of soft, deformable particles within a periodic potential substrate. Moreover, they

*aibq@scnu.edu.cn

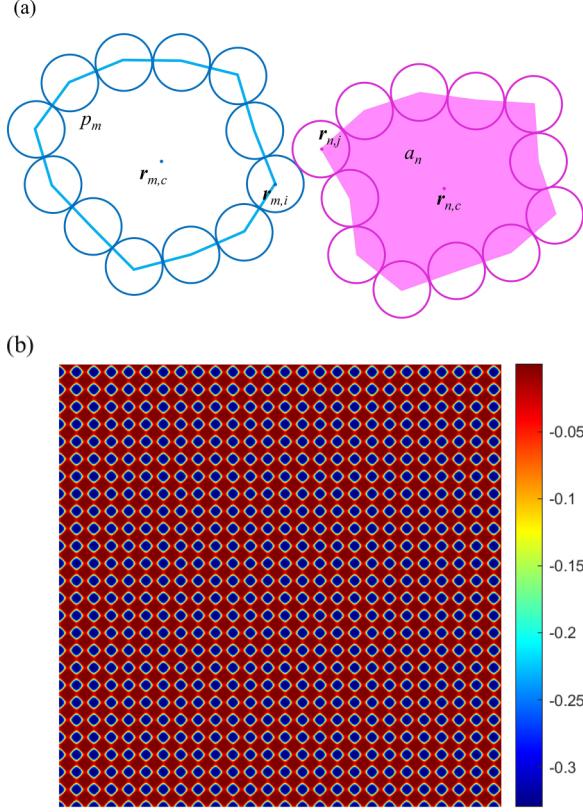


FIG. 1. (a) Illustration of the active deformable particles featuring repulsive interaction. (b) Contour plot showcasing the periodic potential substrate resembling an egg-carton shape.

present a different possibility for sorting active particles based on rigidity differences.

II. MODEL AND METHODS

We consider N deformable particles in a $L \times L$ box where a periodic array of attractive wells exists (shown in Fig. 1). Each deformable particle is a polygon consisting of N_v vertices which represents $N_v - 1$ shape degrees of freedom, and each vertex is a small disk with fixed diameter. The center of mass of the particle m is $r_{m,c} \equiv \{x_{m,c}, y_{m,c}\}$, obtained by the positions of the vertex, and $r_{m,i} \equiv \{x_{m,i}, y_{m,i}\}$ for the vertex i . $l_{m,i} = (r_{m,i+1} - r_{m,i}) = l_{m,i} \hat{l}_{m,i}$ denotes the bond vector between vertex $i+1$ and vertex i . The perimeter of the polygon is $p_m = \sum_{i=1}^{N_v} l_{m,i}$. The internal interaction of such a soft, particulate system is governed by a general shape-energy function [32],

$$\begin{aligned}
 E = & \frac{k_l N_v}{2} \sum_{m=1}^N \sum_{i=1}^{N_v} (l_{m,i} - l_0)^2 + \frac{k_a}{2} \sum_{m=1}^N (a_m - a_0)^2 \\
 & + \sum_{m=1}^N \sum_{n>m}^N \sum_{i=1}^{N_v} \sum_{j=1}^{N_v} \frac{k_r}{2} (l_0 - |r_{m,i} - r_{n,j}|)^2 \\
 & \times \Theta(l_0 - |r_{m,i} - r_{n,j}|), \quad (1)
 \end{aligned}$$

which includes three terms. The first term resists distance fluctuations between two adjacent vertices with moduli k_l

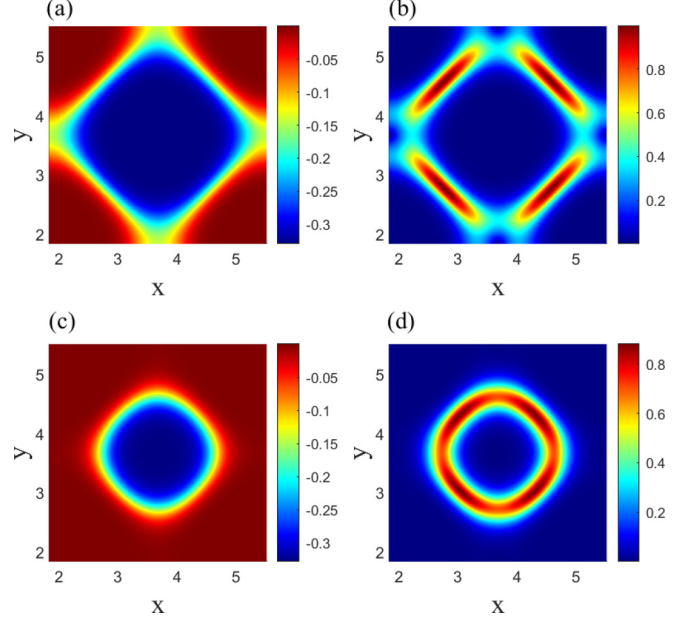


FIG. 2. (a) Contour plot illustrating the potential of the substrate, $U(x, y)$, over a period for $B = 0.025$. (b) Contour plot showcasing the restoring force field derived from (a). (c) Contour plot illustrating the potential of the substrate, $U(x, y)$, over a period for $B = 0.475$. (d) Contour plot showcasing the restoring force field derived from (c). The other parameters are $V_0 = 0.33$, $C = 5.0$, and $\lambda = 3.68$.

and equilibrium length l_0 (also the diameter of each vertex). The second term is a compressibility term quadratic in a_m , resisting area fluctuations with area stiffness moduli k_a , and a_0 is the target area. The last term means a repulsive interaction between polygons when they overlap (i.e., overlapping disks exist on contacting polygons), where k_r is the strength of the repulsive interactions, $r_{m,i}$ is the position of the i th vertex in polygon m , and $\Theta(\cdot)$ is the Heaviside step function. A dimensionless preferred shape parameter $A = (N_v l_0)^2 / (4\pi a_0)$ is introduced to describe the amount of excess perimeter above a regular polygon with area a_0 and to control the deformability of particles [32,37]. Geometrically, $A = 1$ is for a regular circle and $A = 1.16$ is for a regular pentagon. If a polygon with $N_v \rightarrow \infty$ vertices is rigid (regular), $A_v = N_v \tan(\pi/N_v) / \pi \rightarrow 1$. A significant increase in the excess perimeter (the difference between the perimeter and the equilibrium perimeter of the convex hull of each polygon) occurs when $A/A_v > 1.16$ [32], for which the surface tension of the deformable particle decreases as A/A_v increases and the tension is zero at $A/A_v = 1.16$. Therefore, the larger the shape parameter A/A_v , the softer the particles.

The deformable particles are put in a force field (mimic the lattice of optical tweezers) which arises from a two-dimensional (2D) periodic potential [38],

$$U(x, y) = \frac{-V_0}{1 + \exp\left\{-C\left[\cos\left(\frac{2\pi x}{\lambda}\right) + \cos\left(\frac{2\pi y}{\lambda}\right) - 2B\right]\right\}}. \quad (2)$$

V_0 controls the depth of the wells, C controls the steepness, and B controls the relative size of a well with respect to the spatial period λ (shown in Fig. 2).

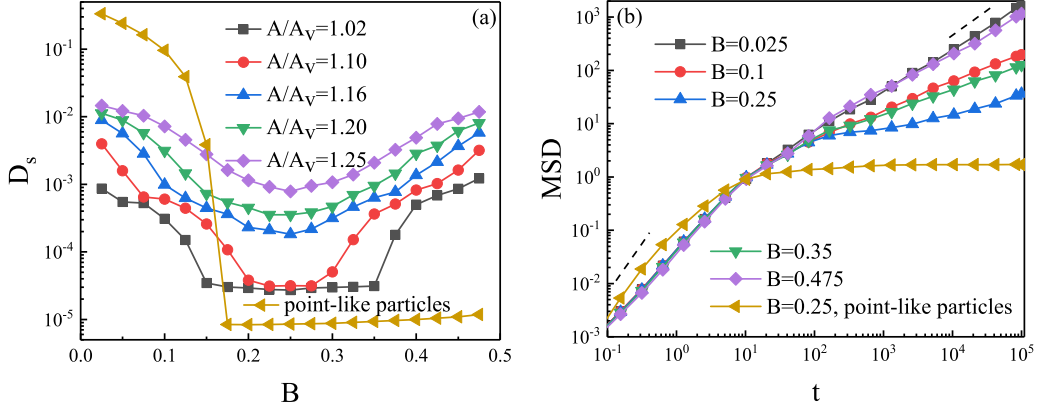


FIG. 3. (a) The self-diffusivity D_s as a function of the parameter B for different shape parameter A/A_v at $v_0 = 0.55$ and $N/N_{\text{trap}} = 1$. (b) The MSD of the centers of mass of the particles for different B at $A/A_v = 1.16$.

To simulate the active deformable particle, we consider a self-propulsion speed $v_{0,m}$ added on the center of mass, and the polarity vector is $n_m = (\cos \theta_m, \sin \theta_m)$. For convenience, we assume that all the deformable particles have the same self-propulsion speed, which is set to be v_0 . The self-propelled velocity needs to be transferred to each vertex because the dynamics equation will be built on the vertices. There are three steps to get the self-propelled velocities on the vertices: (i) calculating the angle between $r_{m,c}$ and $r_{m,i}$ by $\phi_{m,i} = \arctan(\frac{\Delta y_{m,i}}{\Delta x_{m,i}})$, where $\Delta y_{m,i} = y_{m,i} - y_{m,c}$ and $\Delta x_{m,i} = x_{m,i} - x_{m,c}$; (ii) calculating the difference $\Delta \phi_{m,i} = \phi_{m,i} - \theta_m$ and getting its remainder to 2π ; (iii) using formula $v_{0,i} = 0.99v_0 \exp(-\frac{\Delta \phi_{m,i}^2}{2D^2}) + 0.01v_{\text{min}}$ to get the self-propelled velocity component on vertex i . D is the parameter that regulates the precision of the velocity transfer to nearby vertices, and $v_{\text{min}} = 0.01v_0$ ensures that the vertices are active.

The evolution of orientation θ_m is governed by the equation

$$\frac{d\theta_m}{dt} = \sqrt{2D_\theta} \xi_m(t), \quad (3)$$

where D_θ is the rotational diffusion coefficient. $\xi_m(t)$ is a Gaussian white noise with unit variance and zero mean.

In an overdamped regime, the motion of the vertex i of the deformable particle m obeys the following Langevin equation:

$$\frac{dr_{m,i}}{dt} = v_{0,i} n_{m,i} - \mu(\nabla_{m,i} E + \nabla_{m,i} U) + \sqrt{2D_t} \zeta_{m,i}(t), \quad (4)$$

where $n_{m,i} = (\Delta x_{m,i}/\sqrt{\Delta x_{m,i}^2 + \Delta y_{m,i}^2}, \Delta y_{m,i}/\sqrt{\Delta x_{m,i}^2 + \Delta y_{m,i}^2})$ is the orientation of vertex i , and μ is the mobility. $\zeta_{m,i}(t)$ is also a Gaussian white noise.

To study the dynamics behavior of the system, we use the mean square displacement $\text{MSD}(t) = \langle [r_{m,c}(t+t_0) - r_{m,c}(t_0)]^2 \rangle$, where $\langle \cdot \rangle$ denotes an average over all the deformable particles. For the long-time limit, one can obtain the self-diffusivity $D_s = \lim_{t \rightarrow \infty} \frac{\text{MSD}(t)}{4t}$. The appearance of a plateau in the MSD and a very small D_s suggest the disappearance of diffusion, which can be used to distinguish whether deformable particles are trapped in the potential wells qualitatively.

III. RESULTS AND DISCUSSION

A. Zero translational diffusion

In order to investigate the trapping effect of the deformable particles more directly, we first consider the minimal model without translational diffusion ($D_t = 0$). We numerically solved Eqs. (3) and (4) using a stochastic Euler algorithm. The integration time step δt is set to be 0.005 and the total integration time is more than 10^5 . Unless otherwise stated, we set $N = 625$, $N_v = 12$, $\mu = 1$, $D = 1$, $D_\theta = 0.01$, $k_a = 5$, $k_l = 1$, $k_r = 20$, $V_0 = 0.33$, $C = 5$, and $\lambda = 3.68$.

Figure 3(a) illustrates the dependence of self-diffusivity D_s on parameter B for different shape parameter A/A_v at $v_0 = 0.55$. When B increases, D_s first decreases and then increases, and there is a value of parameter B where D_s takes its minimum. Therefore, the deformable particles can be trapped by the wells under intermediate values of parameter B . To obtain the detail information of the evolution of dynamics, we show the MSD as a function of time for different parameter B at $A/A_v = 1.16$. For intermediate values of B (e.g., $B = 0.25$), the MSD exhibits ballistic diffusion (slope close to 2 on a log-log plot) at short times and weak subdiffusion (slope ≈ 0.2) at $t > 10^2$. The subdiffusion indicates that many deformable particles have been caged by the wells. When the B is too small or too large (e.g., $B = 0.025$ or $B = 0.475$), the dynamic behavior of the particles changes from ballistic motion to normal diffusion (slope close to 1 on a log-log plot), so few particles are trapped.

The MSD and D_s can only show a rough picture of the system, but they are difficult to quantitatively identify how many particles are trapped. Therefore, we introduce the fraction of trapped particles (FTP) to accurately evaluate this. The details of the FTP calculation and its robustness are provided in Appendix A. A particle is considered stably trapped if it remains in the same potential well for the last 100τ of the simulation, where $\tau = 1/D_\theta$ is the persistent time. Figure 4 displays the FTP as a function of parameter B for different shape parameter A/A_v at $v_0 = 0.55$. When the shape parameter is large (e.g., $A/A_v \geq 1.16$), the FTP first increases and then decreases with the parameter B , getting its maximum at the intermediate value of B . When the shape parameter is very small (e.g., $A/A_v = 1.02$ and $A/A_v = 1.10$), all of the particles can be stably trapped (FTP = 1) for the intermediate values

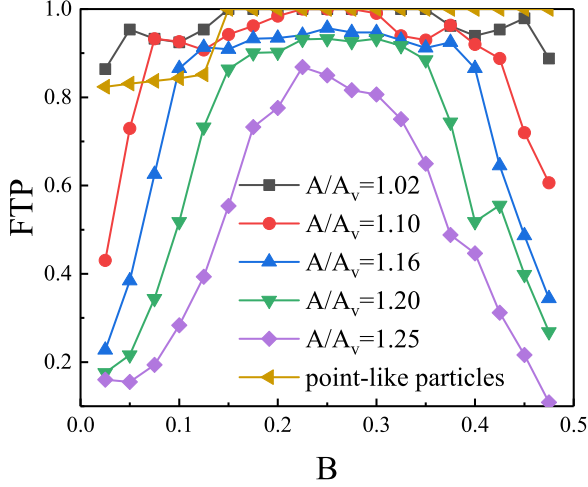


FIG. 4. The fraction of trapped particles (FTP) as a function of the parameter B for different shape parameter A/A_v at $v_0 = 0.55$ and $N/N_{\text{trap}} = 1$.

of parameter B . In particular, there are two additional peaks at either side of the maximum peak.

Now we provide a physical interpretation for the aforementioned phenomena. In order for a particle to cross a potential well, it typically needs to satisfy two conditions: first, the persistence length must exceed the width of the well, and second, the self-propulsion force must surpass the restoring force of the well: in this case, with a persistence length $l_p = v_0/D_\theta = 55$ that is significantly larger than the size of the wells and a self-propulsion force $F_s = v_0/\mu = 0.55$ that is in close proximity to the restoring force at the boundary of the well. When the parameter B is extremely small, the relative size of the wells becomes significantly larger, resulting in a rhombus-shaped potential well with substantial gaps near its four apices. The particles readily escape from such wells [as shown in Fig. 5(a)] and even exhibit normal diffusion behavior ($\text{MSD} \propto t$) after stabilization (e.g., $A/A_v = 1.16$), resulting in a large self-diffusivity (D_s) and small fractional trapping probability (FTP). When the parameter B is significantly increased, the wells noticeably contract, eliminating any gaps and resulting in a slightly higher restoring force near the boundary compared to F_s . Even so, particles still have a slight chance to cross the potential well due to their deformation characteristics. The size of the trap is slightly larger than that of a single particle, but significantly smaller than that of two particles, making it more likely for a trap to be occupied by only one particle. When most of the potential wells already contain one particle each, it becomes difficult for other free particles to find an empty well to occupy. However, if a free particle accidentally enters an occupied well, the collision with the existing trapped particle causes it to be excited out of the trap. As a result, the particles cannot be stably trapped [as shown in Fig. 5(b)] and the FTP is small, leading to normal diffusion after stabilization (e.g., $A/A_v = 1.16$). For intermediate values of parameter B , where the trap size is moderate and the gaps at the top corners are relatively small, the traps can often stably accommodate one or two particles. This results in the maximum FTP and the disappearance of particle diffusion. However, when the shape parameter A/A_v is small

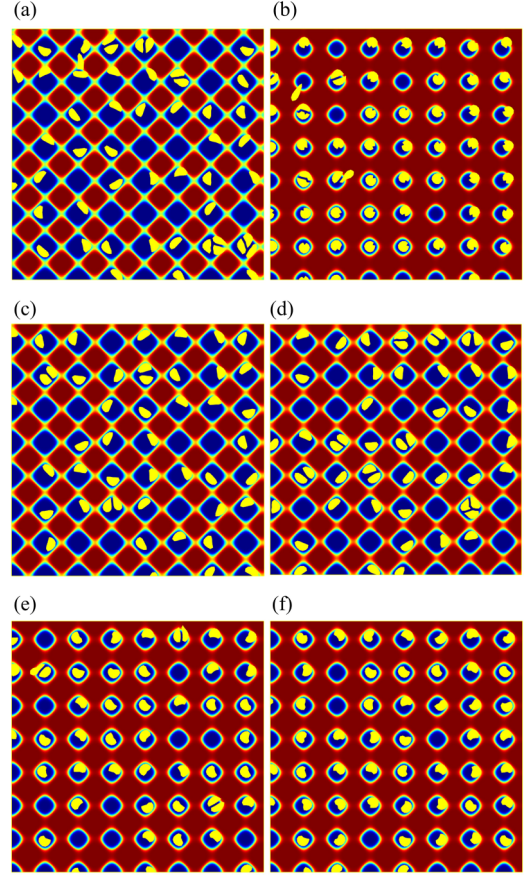


FIG. 5. Typical snapshots of the dynamic behaviors of the active deformable particles for different parameter B : (a),(b) at $A/A_v = 1.16$ and (c)–(f) at $A/A_v = 1.10$. The other parameters are $v_0 = 0.55$ and $N/N_{\text{trap}} = 1$.

($A/A_v < 1.16$), two additional peaks of trapping efficiency are observed. In the subsequent analysis, let us consider the case of $A/A_v = 1.10$ as an example. In the case of the additional peak on the left side, the gaps at the top corners of the traps become narrower as parameter B increases. This narrowing of the gaps facilitates easier trapping of particles [e.g., $B = 0.075$, as shown in Fig. 5(c)]. By further increasing parameter B , smaller gaps allow the traps to transiently accommodate multiple particles (two or three) within certain size limits [e.g., $B = 0.125$, as shown in Fig. 5(d)]. However, the high collision rate among these trapped particles can cause them to become unbound, resulting in a slight decrease in FTP. For the additional peak on the right side, as the parameter B increases [e.g., $B = 0.35$, as shown in Fig. 5(e)], the size of the traps decreases and each trap can no longer stably accommodate multiple particles. The presence of multiple particles within a trap leads to squeezing and collision, causing the particles to escape from the trap and resulting in a slight decrease in the trapping efficiency. With further increases in parameter B , the gaps in the traps narrow, causing the traps to preferentially capture one particle stably, thereby slightly increasing the FTP [e.g., $B = 0.375$, as shown in Fig. 5(f)]. In cases where $A/A_v \geq 1.16$, the particles are sufficiently soft that multiple particles within the same trap tend to be compatible through

deformation rather than being excluded. As a result, there are no additional peaks observed in the FTP.

According to Eq. (2), the size of the trap monotonically decreases with an increase in parameter B , but the D_s and FTP exhibit peak functions (nonmonotonic) of parameter B , which is contrary to intuition. This is the result of the combined effects of the degree of fit between particle size and trap size, and the interactions among particles. When the traps are very large, so are the gaps at their top corners (shown in Fig. 2), allowing the trap to accommodate multiple particles, but not effectively confine them. Conversely, when the traps are very small (for example, only able to accommodate one particle), the high occupancy rate of the traps and the excitation among particles make them difficult to trap a majority of particles. For stiff particles, the FTP even exhibits multiple peaks under the influence of more intense collisions among particles. In short, for intermediate values of parameter B , where the gaps at the top corners of the traps are small and the trap size is moderate, the particles can be more stably trapped.

To gain a more intuitive understanding of the behavior of the aforementioned system, we also calculated the results of active pointlike particles (shape neglected) without repulsive interactions under the same periodic background potential for comparison (shown by the brown lines in Figs. 3 and 4). The details are described in Appendix B. One can observe that the FTP (or D_s) monotonically increases (or decreases) with the increase of parameter B , which is not difficult to envisage. The reduction of the traps (accompanied by the narrowing of the apex gap) causes the boundary restoring force to exceed the self-propulsion force of the pointlike particles. Since the pointlike particles neither have deformation characteristics nor can they overcome the restoring force through interactions with other particles (even though multiple particles may simultaneously exist in a trap), they cannot escape. For instance, when $B = 0.15$, the D_s abruptly transitions to a very small value, and the MSD also exhibits a plateau, indicating a complete disappearance of diffusion behavior. This is compellingly confirmed by $\text{FTP} = 1$. Subsequently, further increasing parameter B , the FTP also remains stably fixed at the value of 1.

Figure 6(a) illustrates the self-diffusivity D_s as a function of the self-propelled velocity v_0 for different values of A/A_v at $B = 0.25$. As $v_0 \rightarrow 0$, the D_s is very small and the MSD exhibits a plateau [e.g., the curve for $v_0 = 0.20$ and $A/A_v = 1.16$ shown in Fig. 6(b)]. This is because the self-propelled force of the particles is too weak to overcome the restoring force of the traps, resulting in most of the particles being trapped. The FTP displayed in Fig. 7 further confirms that all the particles are stably trapped ($\text{FTP} = 1$). As v_0 increases, the self-propelled force also increases, leading to more intense collisions between multiple particles within the same trap. These collisions help the particles escape from the traps and ultimately diffuse freely. Consequently, the self-diffusivity D_s monotonically increases with v_0 . When v_0 is very large (e.g., $v_0 = 0.80$), the MSD scales with time as $\text{MSD} \propto t$, indicating normal diffusion behavior. This is also supported by $\text{FTP} = 0$, indicating that none of the particles are trapped.

Figure 8(a) presents the dependence of the self-diffusivity D_s on the shape index for different values of v_0 at $B = 0.25$. When the self-propelled velocity is very low (e.g., $v_0 = 0.30$),

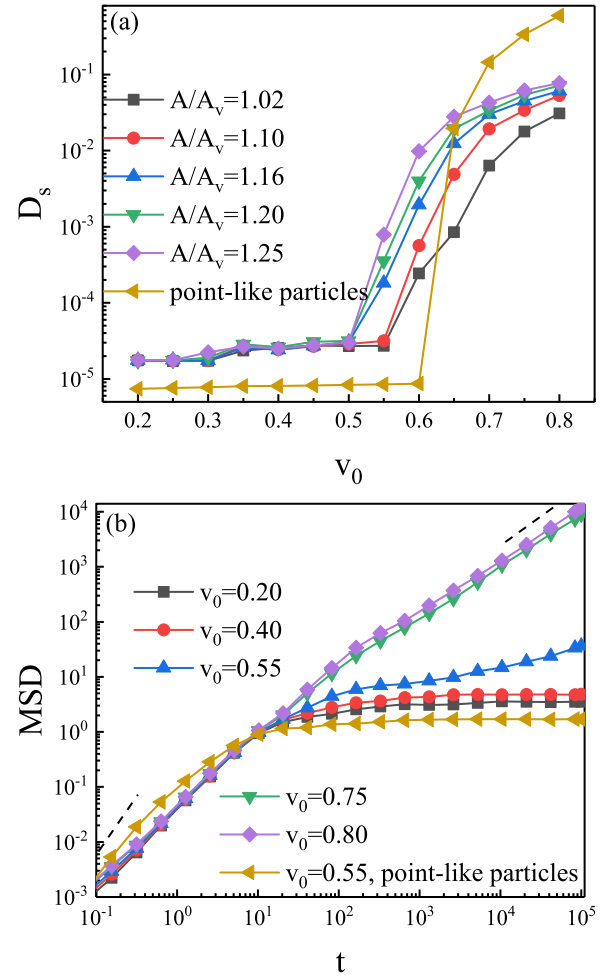


FIG. 6. (a) The self-diffusivity D_s as a function of the self-propelled velocity v_0 for different shape parameter A/A_v at $B = 0.25$ and $N/N_{\text{trap}} = 1$. (b) The MSD of the centers of mass of the particles for different v_0 at $A/A_v = 1.16$.

the particles are unable to overcome the restoring force of the traps. Consequently, regardless of the specific values of A/A_v , the particles remain trapped and no diffusion occurs. For suitable self-propelled velocities, D_s increases monotonically with an increase in the shape index A/A_v . When A/A_v is extremely small (e.g., $A/A_v = 1.02$), there is no diffusion in the system ($D_s \rightarrow 0$) and the MSD exhibits a plateau [as shown in Fig. 8(b)]. The FTP as a function of the shape index A/A_v is depicted in Fig. 9. When A/A_v is very small, the FTP approaches 1, indicating that only a few particles can escape from the traps. When A/A_v becomes very large (e.g., $A/A_v \geq 1.30$), only a small number of particles gets trapped, leading to normal diffusion behavior over long-time regimes ($\text{FTP} \rightarrow 0$). Interestingly, even though the restoring force of the trap boundary under $B = 0.25$ is slightly larger than 0.55 (as shown in Fig. 10), particles with $v_0 = 0.55$ (i.e., $F_s = 0.55$) are still able to escape from the wells. This phenomenon can be explained as follows: as the shape parameter A/A_v increases, the particles become softer and are more likely to undergo deformations. When a particle near the trap boundary deforms such that a part of itself extends outside the trap, the portion outside the trap may exert a dragging force, pulling

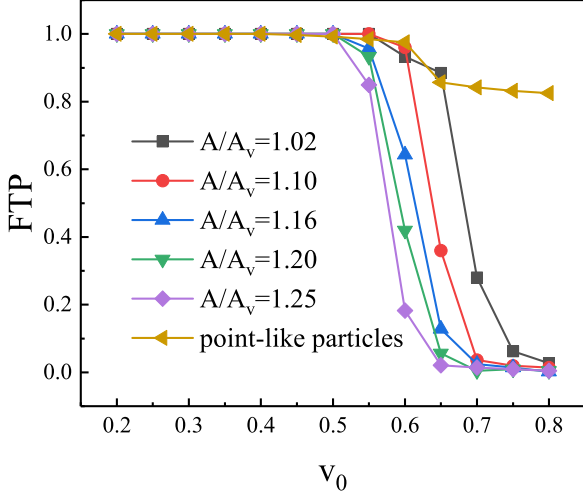


FIG. 7. The FTP as a function of the self-propelled velocity v_0 for different shape parameter A/A_v at $B = 0.25$ and $N/N_{\text{trap}} = 1$.

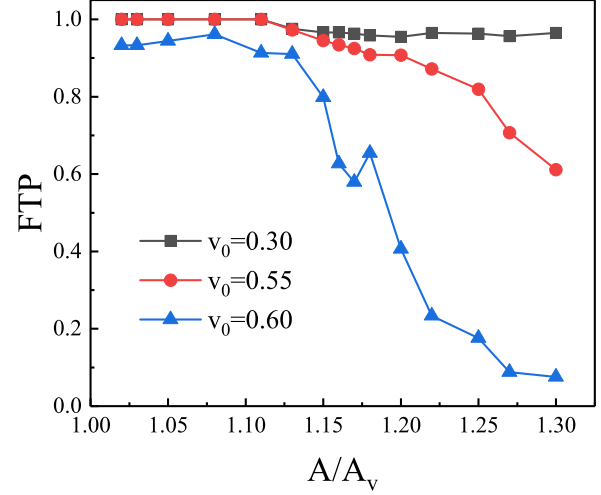


FIG. 9. The FTP as a function of the shape parameter A/A_v for different self-propelled velocity v_0 at $B = 0.25$ and $N/N_{\text{trap}} = 1$.

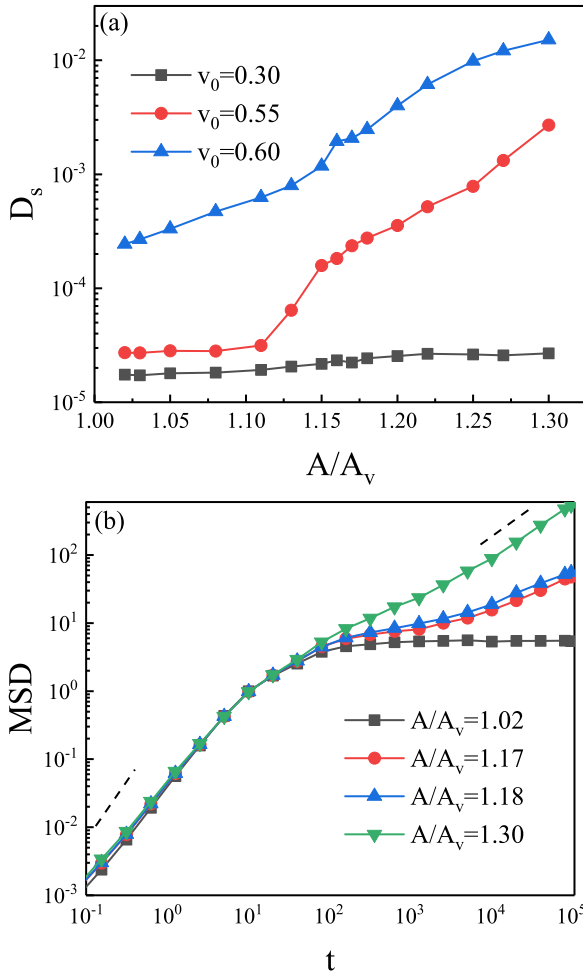


FIG. 8. (a) The self-diffusivity D_s as a function of the shape parameter A/A_v for different self-propelled velocity v_0 at $B = 0.25$ and $N/N_{\text{trap}} = 1$. (b) The MSD of the centers of mass of the particles for different A/A_v at $v_0 = 0.55$.

the entire particle away from the trap. It is worth noting that there is a sharp small valley in the FTP curve when $A/A_v = 1.16$ at large self-propelled velocities (e.g., $v_0 = 0.60$). This is because a zero tension condition allows the particles to rapidly adjust their shape during a vigorous interaction with the trap boundary, facilitating escape from regions with low restoring force. For particles with small v_0 , their interactions with the trap boundary are more gentle, making this effect less noticeable.

In the case of pointlike particles, the loss of deformation characteristics implies that they can only escape from the trap when the self-propulsion force exceeds 0.55 (the boundary restoring force of the traps at $B = 0.25$). Hence, when $v_0 \leq 0.55$, the FTP remains constantly at 1 [shown by the brown line in Fig. 6(b)], and the corresponding MSD also displays a plateau (shown by the brown line in Fig. 7). When $v_0 > 0.55$, the FTP gradually decreases. Note that the FTP cannot decrease to a very small value because the motion of each pointlike particle (i.e., each vertex) is independent and cannot be driven by other pointlike particles (or vertices). Those particles that receive a self-propulsion speed that is less than 0.55 during the transformation of the self-propulsion speed remain in the trap forever.

In order to provide more detailed information regarding the dependence of FTP on the self-propelled velocity v_0 and shape

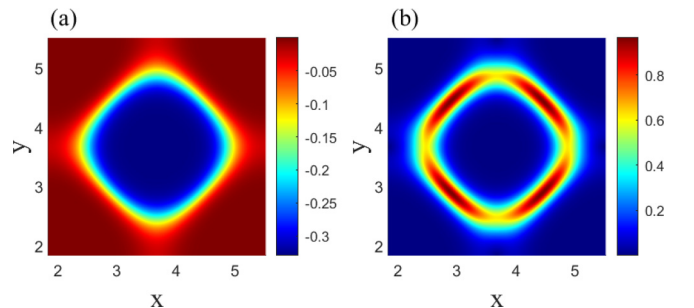


FIG. 10. Contour plots of (a) the potential and (b) the derived restoring force field over a period at $B = 0.25$. Other parameters are $V_0 = 0.33$, $C = 5.0$, and $\lambda = 3.68$.

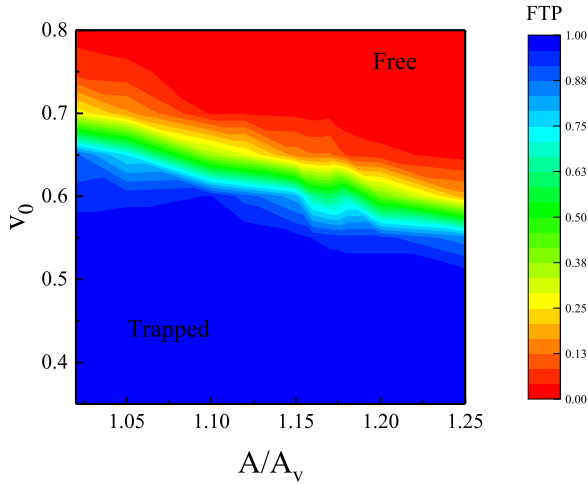


FIG. 11. Phase diagram of the FTP in the $v_0 - A/A_v$ representation at $B = 0.25$ and $N/N_{\text{trap}} = 1$. The background represents the value of FTP according to the color bar on the right.

index A/A_v , we have plotted the phase diagram of FTP on the $v_0 - A/A_v$ panel at $B = 0.25$, as shown in Fig. 11. The phase diagram reveals that decreasing v_0 and A/A_v favors the stable trapping of particles. Additionally, at smaller shape indices, particles require a larger self-propelled velocity to effectively escape from the traps.

Furthermore, we investigate the influence of the ratio of particles to traps, N/N_{trap} , on trapping behaviors. Figure 12(a) illustrates the self-diffusivity D_s as a function of the N/N_{trap} ratio for different A/A_v values at $B = 0.25$. When N/N_{trap} is very small, D_s tends to approach zero, indicating that the particles are trapped. This is supported by the plateau observed in the MSD curve in Fig. 12(b), which signifies the absence of diffusion (e.g., $N/N_{\text{trap}} = 0.5$). As N/N_{trap} increases, D_s monotonically increases, indicating that it becomes progressively more difficult for particles to become trapped. When N/N_{trap} is very large (e.g., $N/N_{\text{trap}} = 2.4$), the particles are completely free and exhibit normal diffusion behavior ($\text{MSD} \propto t$). To further quantify the trapping effect, we plot FTP as a function of N/N_{trap} in Fig. 13. For very small values of N/N_{trap} , FTP tends to approach 1, which demonstrates that all particles are stably

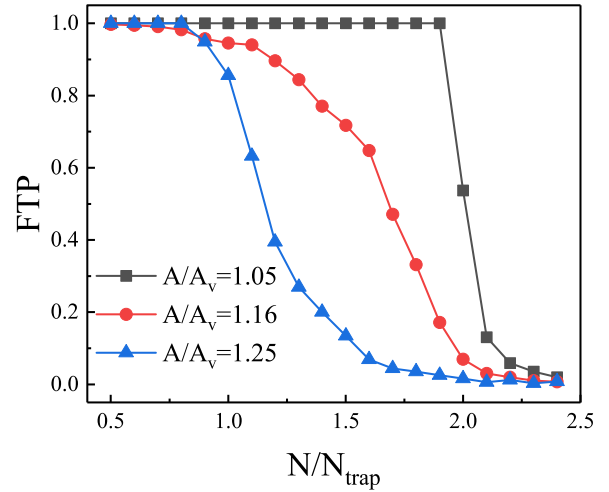


FIG. 13. The FTP as a function of the ratio of the number of particles to traps, N/N_{trap} , for different shape parameter A/A_v at $B = 0.25$ and $v_0 = 0.55$.

trapped. As the N/N_{trap} ratio increases, FTP monotonically decreases from 1 to 0. The above phenomena can be interpreted as follows. When $N < N_{\text{trap}}$, there are enough traps for each particle to occupy individually. Without the assistance of collisions between multiple particles in a trap, it becomes difficult for an individual particle to escape. As the number of particles increases (i.e., when $N/N_{\text{trap}} \geq 1$), multiple particles start occupying a single trap. For stiff particles (e.g., $A/A_v = 1.05$), their limited deformation characteristics make it difficult for them to escape the traps on their own. Additionally, each trap can only accommodate a maximum of two particles due to the trap area being close to the area of two particles. The collision between two particles in a trap does not provide enough force to free the particles when the deformation is weak. Therefore, FTP remains equal to 1 until $N/N_{\text{trap}} \geq 2$. In the case of soft particles (e.g., $A/A_v \geq 1.16$), significant deformations occur, with parts of particles extending outside the traps. This allows the entire particle to be pulled out. On the other hand, the presence of more soft particles within a trap leads to violent collisions between particles that aid in

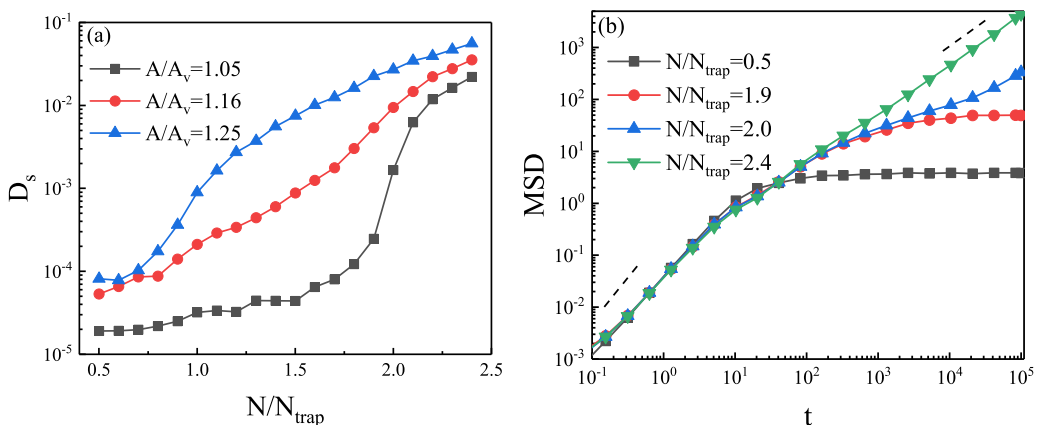


FIG. 12. (a) The self-diffusivity D_s as a function of the ratio of the number of particles to traps N/N_{trap} for different shape parameter A/A_v at $B = 0.25$ and $v_0 = 0.55$. (b) The MSD of the centers of mass of the particles for different N/N_{trap} at $A/A_v = 1.05$.

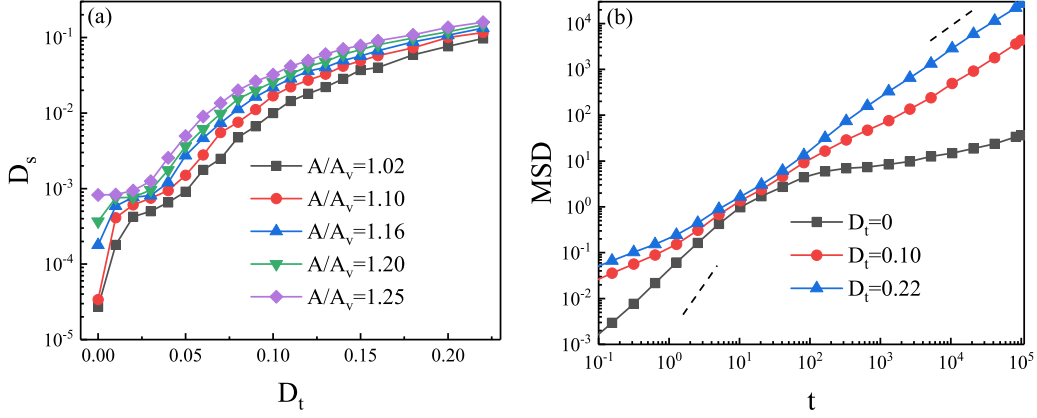


FIG. 14. (a) The self-diffusivity D_s as a function of the translational diffusion coefficient D_t for different shape parameter A/A_v at $B = 0.25$ and $v_0 = 0.55$. (b) The MSD of the centers of mass of the particles for different D_t at $A/A_v = 1.16$.

their escape. Hence, a significant decrease in FTP does not require a large N/N_{trap} ratio for soft particles. When N/N_{trap} is very large, many particles are floating around due to a lack of empty traps. Some of the free particles outside the traps force their way into occupied traps and excite the trapped particles to be released. Consequently, few particles can be stably trapped.

B. The effect of translational diffusion

Translational diffusion is ubiquitous and can have nontrivial effects on the behavior of systems, which should not be neglected. In this section, we study the influence of translational diffusion on trapping of the deformable particles at $v_0 = 0.55$ and $B = 0.25$.

Figure 14(a) depicts the dependence of self-diffusivity D_s on the translational diffusion coefficient D_t for different shape parameter A/A_v . It is found that D_s monotonically increases with an increase in D_t . We analyze the details of the system's dynamic behavior using the case of $A/A_v = 1.16$ as an example, as presented in the MSD shown in Fig. 14(b). When $D_t = 0$, the system exhibits weak subdiffusion over long-time scales, whereas for finite D_t values (e.g., $D_t = 0.10$ and $D_t = 0.22$), the system exhibits normal diffusion. Further calculations of the FTP, plotted as a function of D_t in Fig. 15, show a monotonic decrease with increasing D_t , explicitly indicating that the enhancement of diffusion is caused by the escape of particles from traps. The presence of translational diffusion provides additional kinetic energy for deformable particles to overcome the potential barriers at the trap boundaries. Therefore, the larger the translational diffusion coefficient, the easier it is for particles to escape the confinement of traps.

IV. CONCLUDING REMARKS

In this study, we conducted a numerical investigation into the trapping of active deformable particles in a periodic substrate potential. The findings of our research show that by tailoring parameters such as B (which determines the relative size of wells), self-propelled velocity (v_0), shape parameter (A/A_v), ratio of particles to traps (N/N_{trap}), and translational

diffusion coefficient (D_t), deformable particles can be effectively and stably trapped. The optimal trapping effect occurs with intermediate values of parameter B , as traps that are either too large or too small hinder effective particle trapping. Self-propelled velocity grants particles the necessary active force to resist the restoring force of the traps. Consequently, the higher the self-propelled velocity, the easier particles can escape the traps. Interestingly, softening of the particles can be achieved through an increase in the shape parameter, which facilitates particle escape from the traps, even when the self-propelled force is less than the restoring force. An increase in the translational diffusion coefficient facilitates the escape of the particles from the traps. Furthermore, our study found that the FTP diminishes monotonically as the ratio of particles to traps increases. For rigid particles, even distribution occurs within traps that have an area close to an integer multiple of the particle area. These particles remain stably trapped until N/N_{trap} reaches that multiple. However, with

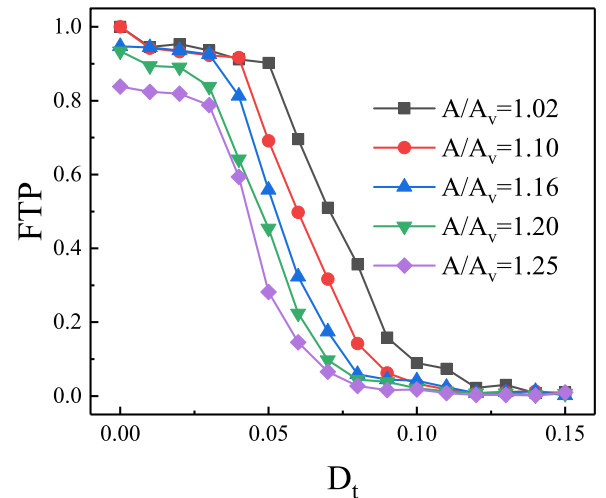


FIG. 15. The FTP as a function of the translational diffusion coefficient D_t for different shape parameter A/A_v at $B = 0.25$ and $v_0 = 0.55$.

softer particles, escape from traps transpires at smaller N/N_{trap} ratios. This research contributes to advancing our understanding of how active deformable particles can be manipulated through a periodic substrate. Additionally, it proposes a different strategy for segregating active particles based on rigidity disparity.

ACKNOWLEDGMENTS

This work was supported in part by the National Natural Science Foundation of China (Grant No. 12075090), the Key-Area Research and Development Program of Guangdong Province (Grant No. 2019B030330001), and the Guangdong basic and applied basic research foundation (Grants No. 2022A1515010449 and No. 2024A1515012575).

APPENDIX A: THE CALCULATION OF FTP

The definition of the fraction of trapped particles (FTP) is the ratio of the number of particles stably trapped to the total number of particles, which reads $\text{FTP} = N_t/N$. Particles that remain trapped in the same traps during the final 100τ ($\tau = 1/D_\theta$) of the simulation time are considered to be stably trapped particles. To confirm that particles stay in the same trap, we need to define a distance Δr_c from the trap center to the trap boundary, where the restoring force at the boundary is equal to the particle's self-propulsion force ($F_s = v_0/\mu$). Due to the shape of the trap not being a regular circle (in fact, it is more akin to a rhombus), we calculate Δr_c by selecting the point that satisfies the restoring force requirement and is the farthest from the trap center within a period. Particles whose displacement is less than Δr_c during the final 100τ are considered to be stably trapped particles. In our simulations, the persistent length $l_p = v_0\tau \geq 20$ is significantly greater than $\Delta r_c \sim 1$, hence it is reasonable to determine whether the particles are trapped by selecting the last 100τ .

To ensure the reliability of our simulation results, we verify the robustness of the FTP in Fig. 16. Figure 16 shows the dependence of FTP on time t for different A/A_v , which indicates that the simulation time of 10^5 is sufficient for the results of the FTP to converge. In other words, our results are not simulation-time dependent.

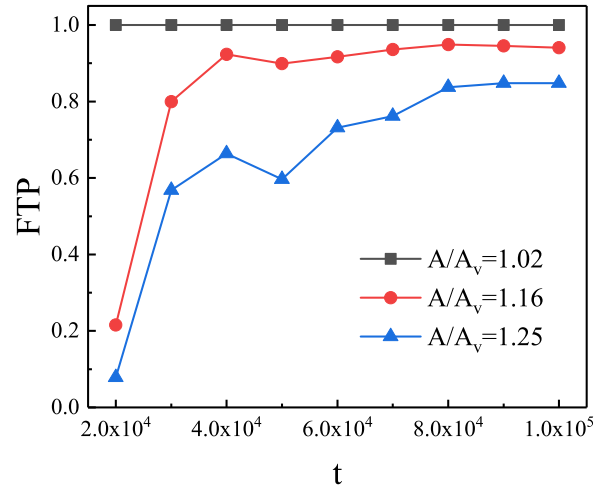


FIG. 16. The FTP as a function of simulation time for different shape parameter A/A_v at $B = 0.25$ and $v_0 = 0.55$.

APPENDIX B: THE SIMULATIONS OF POINTLIKE PARTICLES

To gain a deeper understanding of the system's behavior, we calculate the motion of vertex particles by ignoring the shape constraints of the particles themselves and the repulsive interactions between particles on the basis of the original model, which is equivalent to a simple pointlike particles model. The initial self-propulsion velocity of the point particles is obtained from the velocity transmission mentioned in the main text. Subsequently, the dot particles satisfy the following equations:

$$\frac{dr_i}{dt} = v_{0,i}n_i - \mu\nabla_i U, \quad (\text{B1})$$

$$\frac{d\theta_i}{dt} = \sqrt{2D_\theta}\xi_i(t), \quad (\text{B2})$$

where $n_i = (\cos \theta_i, \sin \theta_i)$ and $i = 1, 2, \dots, N \times N_v$.

The parameters are consistent with those selected in Part A of Sec. III in the main text for comparison with the results of deformable particles.

-
- [1] C. Bechinger, R. Di Leonardo, H. Löwen, C. Reichardt, G. Volpe, and G. Volpe, *Rev. Mod. Phys.* **88**, 045006 (2016).
- [2] R. D. Astumian and M. Bier, *Phys. Rev. Lett.* **72**, 1766 (1994).
- [3] I. Derényi and T. Vicsek, *Phys. Rev. Lett.* **75**, 374 (1995).
- [4] Z. Zheng, G. Hu, and B. Hu, *Phys. Rev. Lett.* **86**, 2273 (2001).
- [5] P. K. Ghosh, V. R. Misko, F. Marchesoni, and F. Nori, *Phys. Rev. Lett.* **110**, 268301 (2013).
- [6] B. Q. Ai, J. Ma, C. H. Zeng, and Y. F. He, *Phys. Rev. E* **107**, 024406 (2023).
- [7] P. Bag, S. Nayak, T. Debnath, and P. K. Ghosh, *J. Phys. Chem. Lett.* **13**, 11413 (2022).
- [8] T. Vicsek, A. Czirók, E. Ben-Jacob, I. Cohen, and O. Shochet, *Phys. Rev. Lett.* **75**, 1226 (1995).
- [9] A. Cavagna, I. Giardina, T. S. Grigera, A. Jelic, D. Levine, S. Ramaswamy, and M. Viale, *Phys. Rev. Lett.* **114**, 218101 (2015).
- [10] L. Berthier, E. Flenner, and G. Szamel, *J. Chem. Phys.* **150**, 200901 (2019).
- [11] E. Flenner, G. Szamel, and L. Berthier, *Soft Matter* **12**, 7136 (2016).
- [12] E. Putzig and A. Baskaran, *Phys. Rev. E* **90**, 042304 (2014).
- [13] E. Mani and H. Löwen, *Phys. Rev. E* **92**, 032301 (2015).
- [14] M. Brun-Cosme-Bruny, A. Förtsch, W. Zimmermann, E. Bertin, P. Peyla, and S. Rafai, *Phys. Rev. Fluids* **5**, 093302 (2020).
- [15] P. Chopra, D. Quint, A. Gopinathan, and B. Liu, *Phys. Rev. Fluids* **7**, L071101 (2022).
- [16] V. Semwal, S. Dikshit, and S. Mishra, *Eur. Phys. J. E* **44**, 20 (2021).
- [17] G. Volpe, I. Buttinoni, D. Vogt, H. J. Kümmerer, and C. Bechinger, *Soft Matter* **7**, 8810 (2011).
- [18] A. Pototsky and H. Stark, *Europhys. Lett.* **98**, 50004 (2012).

- [19] O. Dauchot and V. Démery, *Phys. Rev. Lett.* **122**, 068002 (2019).
- [20] H. E. Ribeiro, W. P. Ferreira, and F. Q. Potiguar, *Phys. Rev. E* **101**, 032126 (2020).
- [21] S. Nayak, S. Das, P. Bag, T. Debnath, and P. K. Ghosh, *J. Chem. Phys.* **159**, 164109 (2023).
- [22] Y. Li, L. Li, F. Marchesoni, D. Debnath, and P. K. Ghosh, *Phys. Rev. Res.* **2**, 013250 (2020).
- [23] T. E. Angelini, E. Hannezo, X. Trepate, M. Marquez, J. J. Fredberg, and D. A. Weitz, *Proc. Natl. Acad. Sci. USA* **108**, 4714 (2011).
- [24] P. Martin and S. M. Parkhurst, *Development* **131**, 3021 (2004).
- [25] G. Katgert and M. van Hecke, *Europhys. Lett.* **92**, 34002 (2010).
- [26] J. Brujić, S. F. Edwards, I. Hopkinson, and H. A. Makse, *Physica A* **327**, 201 (2003).
- [27] E. Mitchell and E. Tjhung, *Soft Matter* **18**, 1082 (2022).
- [28] M. E. Rosti and L. Brandt, *J. Non-Newtonian Fluid Mech.* **262**, 3 (2018).
- [29] D. Wang, J. D. Treado, A. Boromand, B. Norwick, M. P. Murrell, M. D. Shattuck, and C. S. O'Hern, *Soft Matter* **17**, 9901 (2021).
- [30] J. D. Treado, D. Wang, A. Boromand, M. P. Murrell, M. D. Shattuck, and C. S. O'Hern, *Phys. Rev. Mater.* **5**, 055605 (2021).
- [31] C. Brito, H. Ikeda, P. Urbani, M. Wyart, and F. Zamponi, *Proc. Natl. Acad. Sci. USA* **115**, 11736 (2018).
- [32] A. Boromand, A. Signoriello, F. Ye, C. S. O'Hern, and M. D. Shattuck, *Phys. Rev. Lett.* **121**, 248003 (2018).
- [33] D. Cantor, M. Cárdenas-Barrantes, I. Preechawuttipong, M. Renouf, and E. Azéma, *Phys. Rev. Lett.* **124**, 208003 (2020).
- [34] M. Cárdenas-Barrantes, D. Cantor, J. Barés, M. Renouf, and E. Azéma, *Phys. Rev. E* **103**, 062902 (2021).
- [35] Z. Zhang, E. Henry, G. Gompper, and D. A. Fedosov, *J. Chem. Phys.* **143**, 243145 (2015).
- [36] J. J. Li, F. J. Lin, and B. Q. Ai, *New J. Phys.* **24**, 073027 (2022).
- [37] K. VanderWerf, W. Jin, M. D. Shattuck, and C. S. O'Hern, *Phys. Rev. E* **97**, 012909 (2018).
- [38] A. M. Lacasta, J. M. Sancho, A. H. Romero, and K. Lindenberg, *Phys. Rev. Lett.* **94**, 160601 (2005).